Metastable States in Multicomponent Liquid−Solid Systems II: Kinetic Phase Separation

Jan H. Los,* Willem J. P. van Enckevort, and Elias Vlieg

Katholieke Universiteit Nijmegen, Toernooiveld, 6525 ED Nijmegen

Eckhard Flöter and Francois G. Gandolfo

Unilever Research Vlaardingen, Olivier van Noortlaan 120, 3133 AT Vlaardingen

Received: March 6, 2002; In Final Form: May 18, 2002

Compositional kinetic phase separation, indicating the simultaneous growth of solid phases with different compositions during the solification of a mixed system, is investigated on the basis of a relatively simple kinetic model. This model, which has been introduced in a previous paper (Los et al. *J. Phys. Chem. B* **2002**, *106*), is extended with an additional equation describing the evolution of the growth surfaces for the different solid phases. The kinetic model is applied to multicomponent fat mixtures (as model systems) with a focus on phase separation, and the resulting multiple solid, metastable states are compared with the equilibrium predictions. These calculations provide a qualitative, kinetic picture of compositional phase separation during the growth and reveal clearly the role of the undercooling. The extent of the deviations from the equilibrium state are closely related to the phase separation behavior and to the inhomogeneity in the solid phases. For intermediate undercoolings, the kinetically induced reduction of phase separation goes together with an increased inhomogeneity.

1. Introduction

In general, the state of a mixed liquid−solid system is not the equilibrium state, but a metastable state that may persist for long times. The kinetics of the crystallization process may lead to two types of deviations from thermodynamic equilibrium, related to (i) the formation of relatively unstable polymorphs and (ii) the formation of one or more inhomogeneous solid phases, respectively. The formation of the stable polymorphs may be blocked as a result of a high nucleation barrier. As regards the inhomogeneity, the transition to the stable homogeneous situation is prevented by the very low diffusion rate in the solid phase.

This work, which is a continuation of a previous paper,[1] deals with the determination of the metastable states occurring in multicomponent liquid−solid systems by a kinetic modeling of the crystallization process. The usually applied equilibrium approach, which is based on the minimization of the Gibbs free energy[2] and has been described in a concise form in our previous paper, is used as a reference for the results of our kinetic model. Whereas in the previous paper we have restricted ourselves to cases without solid phase separation, here we will particularly focus on systems and conditions that give rise to compositional solid-phase separation, i.e., eutectic or peritectic systems. As model systems we use fat mixtures (blends), as in the previous paper. For many binary fat systems the mixing in the solid phase is far from ideal,[3,4] in contrast to the mixing behavior in the liquid state, which is almost ideal (i.e., zero excess energy).[5]

An example of a eutectic equilibrium phase diagram for a binary system with components A and B is shown in Figure 1a. According to this diagram, below the eutectic temperature T_{eut}, equilibrium thermodynamics predicts two coexisting solid phases in equilibrium with each other, an A-rich and a B-rich solid phase. However, the equilibrium phase diagram gives no direct information about how this equilibrium state is reached. For low cooling rates, usually the following picture is adopted. Assume a completely liquid initial state corresponding to point L_0 in Figure 1a, which is then slowly cooled. Arriving at point L_1 on the equilibrium liquidus, and assuming that no large undercooling is required to form nuclei, a solid phase with a composition corresponding to point S_1 on the equilibrium solidus starts growing. Assuming a finite system, the liquid composition will enrich in component B because of mass conservation. Hence, for continued slow cooling rate the liquid composition will move along the equilibrium liquidus, implying the formation of a solid phase with a composition moving along the equilibrium solidus, until the eutectic point L_{eut} is reached. Then the

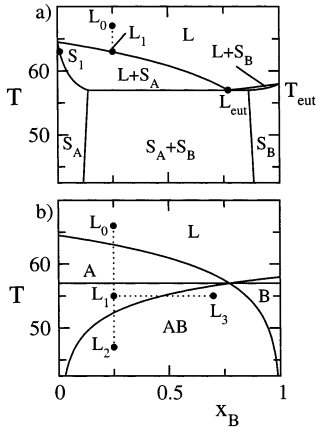

Figure 1. (a) Liquid−solid eutectic equilibrium phase diagram for a binary system with components A and B. (b) Extended equilibrium liquidi for both components with respect to the pure solid phases. The regions A and B denote the regions where the liquid is supersatured for the pure solid phases A and B, respectively. In the region AB the liquid would be supersaturated for both solid phases.

* Corresponding author. E-mail address: janlos@sci.kun.nl.

10.1021/jp0257294 CCC: $22.00
Published on Web 06/21/2002

liquid starts to become supersaturated for the B-rich solid phase, and from that moment the liquid-phase stays at the eutectic point and the A-rich and B-rich solid phases of the eutectic compositions, $S_{eut,A}$ and $S_{eut,B}$, will be formed simultaneously, until the system is completely solidified. It is clear that, if the diffusion in the solid phase is completely neglected, the described crystallization path leads to a final state with an inhomogeneous solid phase; in this particular situation, an inhomogeneous A-rich solid phase. So even in this model, known as the shell model,[6] where the crystallization is assumed to take place slowly and close to equilibrium, the resulting final state is a nonequibrium state.

For high cooling rate, yielding isothermal crystallization conditions far from equilibrium, the shell model does not apply. For example, if a completely liquid system corresponding to L_0 in Figure 1b is cooled to a point L_1 well below the equilibrium temperature, the equilibrium phase diagram does neither give information on the composition(s) of the solid phase(s) that will grow, nor on the number of solid phases (one or two in this case) that will grow at that moment. Actually, extending the solubility curves for each of the two solid phases to the region below the eutectic temperature, as done in Figure 1b, we might expect that from a supersaturated liquid in L_1, which is below the solubility curve for the A-rich solid phase but above that for the B-rich solid phase, only the A-rich solid phase will grow. However, if the liquid is undercooled to a point L_2 in the area AB below both solubility curves, we might expect two simultaneously growing solid phases. In previous work[1,7] this so-called kinetic phase separation has been described by a relatively simple kinetic segregation model, the linear kinetic segregation (LKS) model, which is based on a linear dependence of the mole fraction of a component in the growing solid phase on the supersaturation for that component. However, the LKS model predicts not only kinetic phase separation but also that this phase separation vanishes for increasing undercooling due to kinetically induced mixing. This behavior means that the above discussion on kinetic phase separation on the basis of the extended solubility curves is too simple. That discussion suggests that phase separation is enhanced because of the fact that the separation region, i.e., the horizontal distance between the two solubility curves, gets wider for lower temperatures. Nevertheless, the picture on the basis of the extended solubility curves remains useful as a first guideline for a qualitative understanding of kinetic phase separation. For example, if the crystallization starts for a liquid in L_1, and at that moment the growing solid phase is more rich in component A than the liquid, the liquid will move toward point L_3. It enters the region where we would expect two growing solid phases. This means that after the initial growth of only the A-rich solid phase a second B-rich solid phase will start growing when the concentration of component B in the liquid phase has increased sufficiently. In section 3 it is shown that such situations can indeed occur according to our calculations based on the LKS model.

In literature, the formation of metastable solid solutions after rapid cooling of liquid mixtures is well known.[8] The kinetic segregation taking place at the surface during growth has been investigated by kinetic equation models[9] and discrete Monte Carlo models,[10] usually assuming isothermal conditions, leading to the theoretical determination of kinetic phase diagrams for various materials.[11] However, relatively little attention has been paid to the occurrence of kinetic phase separation and the problems arising from this, such as how to describe the evolution of the growth surfaces for the different growing solid phases. Most of the time, theoretical work on phase separation in solid solutions focuses on the separation process that follows on quenching after the crystallization process has been completed. The subsequent nucleation, growth, and coarsening of the stable domains within the frozen-in metastable solid state, termed Ostwald ripening, with the typical scaling low $L(t)\sim t^{1/3}$ for the size of the domains, has been studied by means of dynamical, statistical mechanical models,[12−14] mostly for 2D binary systems, and Monte Carlo simulations.[15] In contrast, our approach describes the compositional phase separation that occurs during the growth from the fluid motherphase and leads to a final, metastable state that is characterized by the number of final phases and the amounts and average compositions of these phases immediately after the crystallization. In fact, this final state defines properties of an initial state for the models mentioned above, describing the stabilization processes. However, for molecular systems, such as the fat systems used here, where macroscopic transport within the solid phase is negligible, these stabilization processes are very slow and will hardly change the metastable state within a relevant time scale, although some local reordering may occur within days or months for certain systems.[16,17] In our description, mass transport within the solid phase is neglected. Apart from the above-described, compositional kinetic phase separation, also phase separation due to polymorphism may occur. Here we will not consider this type of phase separation, assuming that the primary crystallization process is dominated by the polymorph with the highest growth rate. Furthermore, as in our previous paper, we assume a homogeneous liquid and isothermal conditions during the crystallization. These assumptions, which imply an important simplification of the problem, are justified if the surface incorporation is the rate-limiting process. For fat mixtures this is the case according to refs 18 and 19.

In section 2, after a brief summary of the basic equations of our kinetic model, two models for the evolution of the growth surfaces are proposed and discussed. In sections 3 and 4, the kinetic model is applied to various fat systems with up to eight components. In section 3 various crystallization processes are discussed on the basis of the calculated crystallization curves. In section 4, the metastable states, calculated according to the kinetic model, are compared with the equilibrium predictions.

2. Kinetic Crystallization Model

The previously defined kinetic model,[1] describing the crystallization process in a finite, multicomponent system with N_c crystallizing components and possibly a solvent, consists of the LKS model, represented by the set of $N_c - 1$ equations

$$\frac{x_1^{s,gr}}{x_i^{s,gr}} = \kappa_{1i}\frac{\gamma_1^l x_1^l - \gamma_{1,eq}^{l,gr} x_{1,eq}^{l,gr}}{\gamma_i^l x_i^l - \gamma_{i,eq}^{l,gr} x_{i,eq}^{l,gr}} \quad (i = 2,.., N_c) \qquad (1)$$

and the set of N_c mass conservation equations

$$\frac{dx_i^l}{ds} = \frac{x_i^l - \bar{x}_i^{s,gr}}{1 - s} \qquad (2)$$

where s is the solid fraction of the system, $\boldsymbol{x}^{\mathbf{l}}$ is the liquid composition, and $\bar{\boldsymbol{x}}^{\mathbf{s,gr}}$ is the average instantaneous growth composition of the solid. Here we adopt a vector notation, i.e., by $\boldsymbol{x}^{\mathbf{P}}$ we mean (x_1^P, x_2^P, ...), the subscript referring to the individual components. Note that in this description s is the free variable, and not the time t. This means that the progress of the crystallization process is labeled by the increasing solid fraction s. If $\boldsymbol{x}^{\mathbf{sj,gr}}$ ($j = 1,.., N_s$) are the compositions of the N_s growing solid phases, i.e., all the physically acceptable solutions

(see below) of eq 1, then $\bar{\boldsymbol{x}}^{\mathbf{s,gr}}$ is given by

$$\bar{\mathbf{x}}_{\boldsymbol{i}}^{\mathbf{s,gr}} = \sum_{j}^{N_s} \frac{\mathrm{d}s_j}{\mathrm{d}s} \boldsymbol{x}_{\boldsymbol{i}}^{\mathbf{sj,\,gr}} \tag{3}$$

where $\mathrm{d}s_j$ is the amount of the jth solid that is formed within a small time interval. In eq 1, $\kappa_{1i} \equiv K_{1,0}^{+}/K_{i,0}^{+}$ are kinetic constant ratios. The quantities $\gamma_{i,\mathrm{eq}}^{\mathrm{l,gr}}\, x_{i,\mathrm{eq}}^{\mathrm{l,gr}}$ are related to the pure component thermodynamic proterties. Neglecting small corrections,[1] we have

$$\gamma_{i,\mathrm{eq}}^{\mathrm{l,gr},j}\, x_{i,\mathrm{eq}}^{\mathrm{l,gr},j} = \gamma_i^{\mathrm{sj,gr}}\, x_i^{\mathrm{sj,gr}} \exp\left(-\frac{\Delta H_{i,0}^{\mathrm{sj}}\, \Delta T_i^{\mathrm{sj}}}{R T_i^{\mathrm{sj}} T}\right) \qquad (i = 1,..., N_c, j = 1,.., N_s) \tag{4}$$

for the jth growing solid phase, where T_i^{sj} and $\Delta H_{i,0}^{\mathrm{sj}}$ are the melting temperature and the melting enthalpy, respectively, for the pure component i and the polymorph of the jth solid phase, and $\Delta T_i^{\mathrm{sj}} = T_i^{\mathrm{sj}} - T$ with T the absolute temperature. Adopting the same excess energy model as in ref 1, the so-called three-suffix Margules model[20] extended with an entropy term,[21] the activity coefficients γ_i^P, describing the mixing behavior, are defined in terms of dimensionless excess energy parameters $\phi_{ii'}^{P,\mathrm{exc}}$ for each pair ii'. As in Ref 1, the excess energy parameters were assumed to be independent of the temperature. Ideal mixing implies $\phi_{ii'}^{P,\mathrm{exc}} = 0$ for $i, i' = 1, ..., N_c$, whereas two components i and i' tend to separate if $\phi_{ii'}^{P,\mathrm{exc}}$ is large (and positive).

The growth rate for the jth growing solid phase, R^{sj}, is equal to the sum of the growth rates for the individual components, R_i^{sj}, i.e.,

$$R^{\mathrm{sj}} = \sum_{i=1}^{N_c} R_i^{\mathrm{sj}} = \sum_{i=1} K_{i,0}^{+} (\gamma_i^{\mathrm{l}}\, x_i^{\mathrm{l}} - \gamma_{i,\mathrm{eq}}^{\mathrm{l,gr},j}\, x_{i,\mathrm{eq}}^{\mathrm{l,gr},j}) \tag{5}$$

where $K_{i,0}^{+}$ (in $\mathrm{m}^{-2}\ \mathrm{s}^{-1}$) is the attachment probability per unit surface area for growth in a pure system of component i.

A solution $\boldsymbol{x}^{\mathbf{sj,gr}}$ of eq 1 is physically acceptable if all $R_i^{\mathrm{sj}} > 0$ and if it corresponds to a stable steady-state solution. In ref 1 it was shown that a solution of eq 1 is a steady-state solution of a first order differential equation, which is stable if the real parts of all the eigenvalues of the Jacobian of the vector function $\boldsymbol{F}(\boldsymbol{x}^{\mathbf{s,gr}}) \equiv (\boldsymbol{R} - R\boldsymbol{x}^{\mathbf{s,gr}})$ at the solution, i.e., $\mathrm{d}\boldsymbol{F}/\mathrm{d}\boldsymbol{x}^{\mathbf{s,gr}}|_{\boldsymbol{x}^{\mathrm{sj,gr}}}$, for eigenvectors belonging to the invariant subspace defined by $\sum_i x_i^{\mathrm{s}} = 1$, are negative. Solutions that do not satisfy this stability condition will not grow as bulk phases and should be discarded.

To be able to solve the above set of equations, along with the stoichiometric conditions $\sum_i x_i^{\mathrm{sj,gr}} = 1$ ($j = 1, .., N_s$), for the case that more than one solid phases are formed, one needs to know the relative growth fractions $\mathrm{d}s_j/\mathrm{d}s$ in eq 3. The amount (in moles) of the jth solid phase, $\mathrm{d}S_j$, that is formed in a small time interval, $\mathrm{d}t$, is given by

$$\mathrm{d}S_j = R^{\mathrm{sj}} A^{\mathrm{sj}}\, \mathrm{d}t \tag{6}$$

where A^{sj} is the growth surface for the jth solid. The total amount of solid phase, $\mathrm{d}S$, that is formed in the time interval $\mathrm{d}t$ is equal to

$$\mathrm{d}S = \sum_j \mathrm{d}S_j = \sum_j R^{\mathrm{sj}} A^{\mathrm{sj}}\, \mathrm{d}t \tag{7}$$

Using the fact that $\mathrm{d}s_j/\mathrm{d}s = \mathrm{d}S_j/\mathrm{d}S$, we find

$$\frac{\mathrm{d}s_j}{\mathrm{d}s} = \frac{R^{\mathrm{sj}} A^{\mathrm{sj}}}{\sum_j R^{\mathrm{sj}} A^{\mathrm{sj}}} = \frac{R^{\mathrm{sj}} a^{\mathrm{sj}}}{\sum_j R^{\mathrm{sj}} a^{\mathrm{sj}}} \tag{8}$$

where $a^{\mathrm{sj}} = A^{\mathrm{sj}}/(\sum_j A^{\mathrm{sj}})$ is the growth surface fraction for the jth solid phase. The determination of the evolution of these growth surface fractions is a complex problem. Two approaches are now described and discussed.

Evolution of the Growth Surfaces. The most simple approach would be to neglect the history of the evolution of the growth surfaces during crystallization completely by taking all growth surface fractions equal to each other, i.e., $a_{\mathrm{s}1} = a_{\mathrm{s}2} = ... = 1/N_s$. One could say that at each moment the total growth surface is equally "shared" by the different growing solid phases. Then, according eq 8, the relative growth fractions $\mathrm{d}s_j/\mathrm{d}s$ are given by

$$\frac{\mathrm{d}s_j}{\mathrm{d}s} = \frac{R^{\mathrm{sj}}}{\sum_j R^{\mathrm{sj}}} \tag{9}$$

Hence, in this approach the ratio of the relative growth fractions is just equal to the ratio of the actual growth rates. We will refer to this as the "no-history model".

In the following derivation of the second, more sophisticated model for the evolution of the growth surfaces we will for convenience assume only two growing solid phases. The derivation for the case with more than two solid phases is very similar, and the result will be given at the end of this section.

If there would be only one growing solid phase, then the growth surface A for this solid phase could be written as

$$A = \Omega_{\mathrm{d}} \sum_l r_l^{(d_{\mathrm{cr}}-1)} \tag{10}$$

where r_l is the radius of the lth crystallite and the sum runs over all crystallites. The dimension d_{cr} is an effective dimension related to the geometry of the crystallites, and Ω_{d} is the corresponding geometrical factor. For spherical crystallites $d_{\mathrm{cr}} = 3$ with $\Omega_3 = 4\pi$; for circular plate-like crystallites, where the growth only occurs at the borders of the plates, $d_{\mathrm{cr}} = 2$ and $\Omega_2 = 2\pi$. We note that the value of this effective dimension may not be an integer for cases where the crystallites are neither completely spherical nor plate-like, and that correspondingly the value of Ω_{d} will have an intermediate value. The rate of change of A can be written as

$$\frac{\mathrm{d}A}{\mathrm{d}t} = (d_{\mathrm{cr}} - 1)\Omega_{\mathrm{d}} \sum_l r_l^{(d_{\mathrm{cr}}-2)} \frac{\mathrm{d}r_l}{\mathrm{d}t} \equiv \frac{g\Omega}{\tilde{r}} RA \tag{11}$$

where R is the growth rate according to eq 5 and we have used that $\mathrm{d}r_l/\mathrm{d}t = V_{\mathrm{p}}R$ for all crystallites, with V_{p} the volume of one growth unit. The length $\tilde{r}$ is of the order of the average radius of the crystallites such that $\sum_l \tilde{r} r_l^{(d_{\mathrm{cr}}-2)} = \sum_l r_l^{(d_{\mathrm{cr}}-1)} = A/\Omega_{\mathrm{d}}$ and $g = d_{\mathrm{cr}} - 1$ is a geometrical factor. In principle, $\tilde{r}$ is time dependent. We note that eq 11 does not contain a term that explicitly takes into account the increase of the number of crystallites due to homogeneous nucleation. Initially, the radius of new nuclei is very small and so their contribution to the total growth surface is negligible. However, the formation of the new nuclei has an effect on the average radius, $\tilde{r}$, so that its

contribution to dA/dt is implicitly included in the factor $1/\tilde{r}$ in eq 11. Likewise, also the aggregation of crystallites, leading to an increase in the average radius $\tilde{r}$, is assumed to be included in the factor $1/\tilde{r}$.

For the case that there are two growing solid phases with different growth compositions and growth rates R^{s1} and R^{s2} we propose the following expression for the evolution of the growth surfaces:

$$\frac{dA^{sj}}{dt} = \frac{gV_p}{\tilde{r}}(R^{sj}A^{sj} + \nu_{jj'}R^{sj}A^{sj'} - \nu_{j'j}R^{sj'}A^{sj}) \quad (j = 1, 2; j' \neq j) \quad (12)$$

where the second and third terms on the right-hand side account for the heterogeneous nucleation of solid phase j on the growth surface for the j'th solid phase and for the nucleation of solid phase j' on the growth surface for the jth solid phase, respectively. For eq 12 we have implicitly assumed that both solid phases occur as domains in common polycrystallites, so that there is still one average radius $\tilde{r}$. This assumption is supported by the fact that, in general, the heterogeneous nucleation rate is much larger than homogeneous nucleation rate. Both the parameter g and the nucleation parameters $\nu_{jj'}$ are dimensionless. The nucleation parameters $\nu_{jj'}$ express the fact that the growth rate of a solid phase j onto the growth surface for the j'th solid phase will be less than the growth rate on its own growth surface, so that we may assume that $\nu_{jj'} < 1$. The rate of change of the growth surface fraction is given by

$$\frac{da^{sj}}{dt} = \frac{d(A^{sj}/A)}{dt} = \frac{A^{sj'}}{A^2}\frac{dA^{sj}}{dt} - \frac{A^{sj}}{A^2}\frac{dA^{sj'}}{dt} \quad (j' \neq j) \quad (13)$$

where $A = A^{s1} + A^{s2}$ is the total growth surface. Substitution of eq 13 into eq 12 leads to

$$\frac{da^{sj}}{dt} = \frac{gV_p}{\tilde{r}}((\nu^+_{jj'}R^{sj} - \nu^+_{j'j}R^{sj'})a^{s1}a^{s2} + \nu_{jj'}R^{sj}(a^{sj'})^2 - \nu_{j'j}R^{sj'}(a^{sj})^2) \quad (14)$$

where $\nu^+_{jj'} \equiv 1 + \nu_{jj'}$. To express the evolution of a^{sj} as a function of the solid-phase fraction s, we use $da^{sj}/ds = (da^{sj}/dt)/(ds/dt)$, which, in combination with

$$\frac{ds}{dt} = \frac{1}{L+S}\frac{dS}{dt} = \frac{R^{s1}A^{s1} + R^{s2}A^{s2}}{L+S} = \frac{A}{L+S}(R^{s1}a^{s1} + R^{s2}a^{s2}) \quad (15)$$

leads to

$$\frac{da^{sj}}{ds} = \frac{gV_p(L+S)}{\tilde{r}A} \times \left(\frac{(\nu^+_{jj'}R^{sj} - \nu^+_{j'j}R^{sj'})a^{s1}a^{s2} + \nu_{jj'}R^{sj}(a^{sj'})^2 - \nu_{j'j}R^{sj'}(a^{sj})^2}{R^{s1}a^{s1} + R^{s2}a^{s2}}\right) \quad (16)$$

where L and S are the total amounts (in moles) of the liquid and the solid phase, respectively. The value of $\tilde{r}A$ is of the order of $d_{cr}V_s$ where V_s is the volume occupied by the solid phase. This implies $V_p(L+S)/(\tilde{r}A) \simeq (L+S)/(d_{cr}S) = 1/(d_{cr}s)$ for the prefactor in eq 16. Although this reasoning is correct for small solid fraction s, it is incorrect for a high solid phase fraction due to an enhanced aggregation of the crystallites, leading to a reduction of the growth surface at the contact boundaries. For high solid fraction, the growth surface would be related to the average size of the liquid holes rather than to the size of the crystallites. If $\tilde{r}$ was the average radius of the liquid holes, then the prefactor would be proportional to $1/l = 1/(1-s)$ in the same way as we have derived the prefactor $1/s$ above. Therefore, as a compromise, the prefactor is set equal to $1/(s(1-s))$, which gives the right behavior for $s \to 0$ and $s \to 1$. Furthermore, the nucleation parameters, for which no accurate values are available, will be assumed equal to each other, i.e., $\nu_{12} = \nu_{21} \equiv \nu$. All together this leads us to the following expression for da^{sj}/ds:

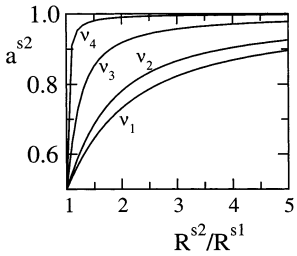

Figure 2. The steady-state value of the growth surface fraction for the solid phase 2, a^{s2}, according to eq 17 for the case of two growing solid phases, as a function of the ratio of the growth rates R^{s2}/R^{s1} for values of the nucleation parameter ν equal to $\nu_1 = 1$, $\nu_2 = 0.5$, $\nu_3 = 0.1$, and $\nu_4 = 0.01$.

$$\frac{da^{sj}}{ds} = \frac{g}{s(1-s)} \times \left(\frac{\nu^+(R^{sj} - R^{sj'})a^{s1}a^{s2} + \nu R^{sj}(a^{sj'})^2 - \nu R^{sj'}(a^{sj})^2}{R^{s1}a^{s1} + R^{s2}a^{s2}}\right) \quad (17)$$

where $\nu^+ \equiv 1 + \nu$ and we have redefined $g = (d_{cr} - 1)/d_{cr}$, so that $g \in (0.5, 1)$.

In view of the rather crude approach in the derivation of eq 17, let us discuss whether this equation makes any sense. Generally speaking, the effect of eq 17 is such that the system develops toward a situation where the growth surface for the solid phase with the largest growth rate will dominate, as to be expected. Eventually a steady state will be reached, where $da^{s1}/ds = da^{s2}/ds = 0$. In Figure 2 the steady-state value of a^{s2} is shown as a function of R^{s2}/R^{s1} for various values of ν, calculated by solving eq 17 for $da^{sj}/ds = 0$. Note that the steady state value depends only on ν and not on g. For $R^{s1} = R^{s2}$ we find $a^{s1} = a^{s2} = 1/2$ as it should be, but for the case that $R^{s2} > R^{s1}$ the steady-state value of a^{s2} rapidly tends to 1 for small values of ν.

Imagine a situation where initially only one solid phase, say solid phase 1, is growing. Then, suppose that at a given moment the liquid composition has changed such that a second solid phase starts growing with, at that momemt, a larger growth rate than the first one, i.e., $R^{s2} > R^{s1}$. That such a situation can actually occur will be shown in section 3. At the moment that the second solid phase starts growing, we have $a^{s1} = 1$ and $a^{s2} = 1 - a^{s1} = 0$, but according to eq 17 we also have $da^{s1}/ds < 0$ and $da^{s2}/ds = -da^{s1}/ds > 0$ due nucleation terms. Hence, the growth surface for the second solid starts to develop. As soon as a^{s2} is not zero anymore, a^{s2} starts to increase more rapidly due to the first term on the right-hand side and stays increasing, at least as long as $R^{s2} > R^{s1}$, until eventually a steady state is reached where $a^{s2} \gg a^{s1}$. The rate of the here-described transition in the growth surface fractions for given R^{s1} and R^{s2} depends, according to eq 17, on s and on the values of both g and ν. For small s, da^{sj}/ds is approximately proportional to $1/s$. Hence, the transition rate decreases for increasing solid fraction,

as expected. The larger the amount of solid, the larger the growth surface and the larger is the amount of solid needed to cover this growth surface by a different solid phase. The opposite holds for solid fractions close to one, where da^{sj}/ds is approximately proportional to $1/(1 - s)$. Furthermore, the larger the values of g and ν, the faster is the transition. A large ν implies a fast heterogeneous nucleation of one solid phase onto the other, favoring a fast transition of the growth surfaces.

We thus conclude that, qualitatively, eq 17 contains correct dependencies and describes a behavior that intuitively makes sense. However, it contains two parameters that are not very well known. This holds in particular for the nucleation parameter ν, but also the value of the geometrical factor g could differ from the above given approximation for certain cases where the assumptions made in the derivation of eq 17 may not be valid or may be only partly valid. Nevertheless, eq 17 with values for g and ν within reasonable domains can very well be used as a tool in studying the influence of the evolution of growth surfaces in a crystallization process with kinetic phase separation. Future work will be addressed to possible improvement of this growth surface model and to retrieve more accurate values for the occurring constants. For the more general case with N_s growing solid phases, a similar derivation, assuming again that $\nu_{jj'} = \nu$ for all $j, j' = 1, .., N_s$, leads to

$$\frac{da^{sj}}{ds} = \{g\sum_{j'\neq j}[\nu^{+}(R^{sj} - R^{sj'})a^{sj}a^{sj'} + \nu(\sum_{j''\neq j}R^{sj}a^{sj'}a^{sj''} - \sum_{j''\neq j'}R^{sj'}a^{sj}a^{sj''})]\}/s(1-s)\sum_{j}R^{sj}a^{sj} \quad (18)$$

where $g \in (0.5, 1)$ and $\nu^{+} = 1 + \nu$ as defined above. It is easy to check that for $N_s = 2$ eq 18 becomes equivalent to eq 17. Qualitatively, the behavior described by eq 18 for $N_s > 2$ is the same as for $N_s = 2$. In the steady-state regime the character of the growth surface will be dominated by the solid phase with the largest growth rate.

The complete set of coupled eqs 1, 2, 3, 4, 8, and 18 (or for the "no-history model" eq 9 instead of eqs 8 and 18) together with the required expression for the $\gamma_{i,eq}^{sj,gr}$ in terms of $\boldsymbol{x}^{sj,gr}$ from ref 1 and the stoichiometric condition $\sum_i x_i^{sj,gr} = 1$, can be solved numerically. Details on the numerical solution method and the corresponding software we have developed for it may be given elsewhere. For the calculations in the next sections, following ref 5, the mixing behavior in the liquid was assumed to be ideal, i.e., $\phi_{ii'}^{l,exc} = 0$ for all pairs ii'. All kinetic constants $K_{i,0}^{+}$ were taken equal to 1 assuming an appropriate time unit. The remaining thermodynamic data for the systems used are given in Appendix A. The reference undercooling used in the next section is defined as $\Delta T_0 = T_{eq,max} - T$, where $T_{eq,max}$ is the equilibrium temperature for the system consisting of $(1 - z_{solv})$ moles of the component with the largest T_i and z_{solv} moles of the solvent. Note that the real undercooling changes during crystallization of mixed systems at constant T.

As already mentioned, our model is defined in terms of the solid fraction. A connection with the evolution of the crystallization process in time, which would be desirable for the comparison with experimental data as a function the applied cooling rate, can be obtained most conveniently by eq 7 and using $A^{sj}(s) = a^{sj}(s)A(s)$. The total growth surface $A(s)$ is related to the averaged size of the crystallites that could be obtained from the experiment as a function of the measured $s(t)$.

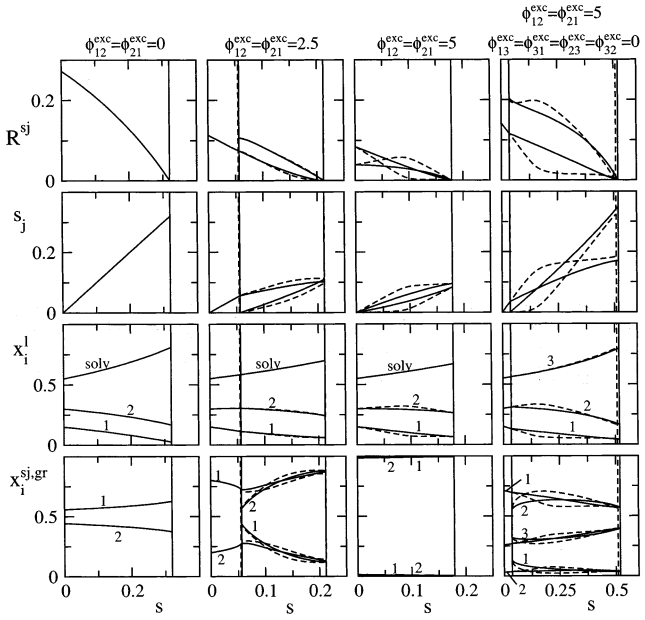

Figure 3. Crystallization curves representing the evolution of a crystallization process for the binary system PPP−MyPP plus a solvent with overall mole fractions $z = (0.15, 0.30)$, implying $z_{solv} = 0.55$ (graphs in the first three columns), and the ternary system PPP−MyPP−SOS with overall mole fractions $z = (0.15, 0.30, 0.55)$ (graph in the last column). The graphs in the first three columns are for different settings of the excess energy parameters, as indicated above the top graphs. The full lines represent the results using the "no-history model" (eq 9). The dashed lines are the results using the growth surface model eq 17 with $g = 1$ and $\nu = 0.01$. The crystallization temperature was taken equal to $T_{cr} = 323$ K in all three cases.

3. Multiple Crystallization Curves

In ref 1 we have presented crystallization curves for cases where only one solid phase was formed. These curves gave the evolutions of R^s, x_i^l, and x_i^s as a function of the solid fraction s. For cases where kinetic phase separation takes place, more than one solid phase is formed and correspondingly we have multiple crystallization curves, giving the evolutions of R^{sj}, s_j, and x_i^{sj} for each of the $j = 1, ..., N_s$ solid phases as a function of s $(= \sum_j s_j)$.

Examples of multiple crystallization curves are shown in Figure 3 for a system with two crystallizing components, PPP and MyPP, with overall mole fractions $z_1 = 0.15$ and $z_2 = 0.30$, respectively, and a solvent with overall mole fraction $z_{solv} = 0.55$, and the ternary system PPP−MyPP−SOS with overall fractions $\boldsymbol{z} = (0.15, 0.30, 0.55)$. Here we adopted the conventional nomenclature for the triglycerides (fat molecules), as specified in Appendix A. The crystallization temperature was taken equal to $T_{cr} = 50$ °C, which for the binary system plus solvent is about 6 degrees below the eutectic temperature in the limit of pure solid phases. We will first discuss the results obtained by using the "no-history model" (eq 9) for the determination of ds_j/ds, represented by the full lines.

For ideal mixing, i.e., $\phi_{21}^{s,exc} = \phi_{12}^{s,exc} = 0$, no kinetic phase separation occurs. In that case there is only one set of curves. The bottom graph shows that the solid is well mixed in this case. For $\phi_{21}^{s,exc} = \phi_{12}^{s,exc} = 2.5$ mixing becomes energetically less favorable and two phases are formed. Initially, only one solid phase is growing, but at a solid fraction equal to $s \simeq 0.055$, marked by the left vertical line, a second solid phase starts growing, which at that moment has a larger growth rate than the first one. As a result of this, the increase of the fraction s_2

of the second solid phase is larger than that of s_1, and at the end of the crystallization process, marked by the right vertical line, almost an equal amount of each solid phase has been formed, as can be seen in the second graph from above. When the growth stops, the remaining liquid and the last grown fractions of each of the two solid phases have approximately the eutectic compositions. The bottom graph shows that, roughly speaking, one of the solid phases is rich in component 1 (PPP), whereas the other solid phase is rich in component 2 (MyPP). However, note that at the moment that the second solid phase starts growing, the growth composition of this phase is well mixed. As the crystallization process proceeds and the supersaturation decreases, the growth compositions of both solid phases become less mixed. This effect of a decreasing supersaturation on the mixing behavior is in agreement with the kinetic phase diagrams presented previously for binary fat mixtures.[1,7] For $\phi_{21}^{s,exc} = \phi_{12}^{s,exc} = 5$, two solid phases start growing immediately for the binary system plus solvent. In this case the separation tendency is so strong that two almost pure solid phases are formed. Apparently, in this case the chosen crystallization temperature is not low enough to allow for an enhanced, kinetically induced mixing. For the ternary system, where the solvent in the previous system is replaced by a third crystallizing component (SOS), again two solid phases are formed. The second solid phase starts to grow soon after the first one, i.e., at a low solid phase fraction. The mixing of components 1 and 2 in the solid phase has increased significantly as compared to the binary system plus solvent with the same excess energy parameters for these components. This is due to the good miscibility of components 1 and 2 with component 3, for which all the excess energy parameters are taken equal to zero in this case. The presence of the third component, with a fraction of around 0.3 in the solid phase, dilutes the solid solution of components 1 and 2, reducing the mixing excess energy. This argument applies generally to multicomponent systems. The high miscibility of a subset of components facilitates the mixing of the other low mixing components.

The dashed lines in Figure 3 represent the results using the growth surface model eq 17 with $g = 1$ and $\nu = 0.01$. For $\phi_{21}^{s,exc} = \phi_{12}^{s,exc} = 2.5$, initially only one solid phase is growing, which is rich in PPP (see bottom graph). Of course then the dashed and full line overlap, but when the second solid phase starts to grow, and the evolution of the growth surfaces starts to play a role, differences occur although these are rather small in this case. For the same system but $\phi_{21}^{s,exc} = \phi_{12}^{s,exc} = 5$, where two solid phases start growing immediately, initially the growth rate of one solid phase, say solid phase 1, is about twice as large as that of solid phase 2. Therefore, the growth surface of solid phase 1 will dominate and so the formation of the solid phase proceeds most rapidly in the beginning as is shown by the evolution of the s_j (second graph from above). Consequently, the supersaturation for solid phase 1 decreases while that of solid phase 2 increases, so that at a certain moment both growth rates cross. From that moment the growth surface for solid phase 2 starts to evolve more rapidly according to eq 17 and at the end of the crystallization process the fractions of both solid phases are equal to those found using the "no-history model".

Basically the same reasoning holds for the ternary system. We note that the total solid-phase fraction for the binary system plus solvent according to our kinetic model must be equal to the equilibrium solid fraction, since it is determined by the eutectic point, which is the end point of the crystallization. This is independent of the growth surface model and the values of the parameters in this model. However, for a ternary system

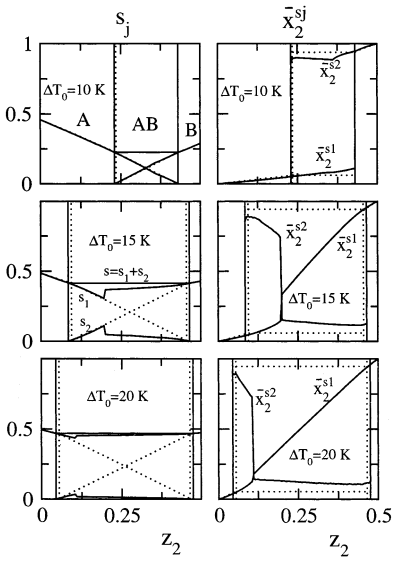

Figure 4. Characterization of the metastable (full lines) and the equilibrium states (dotted lines) for the crystallization of the binary mixture PPP−MyPP as a function of the overall mole fraction z_2 of component 2 (MyPP) with a fixed overall solvent fraction $z_{solv} = 0.5$, implying $z_1 = z_{PPP} = 0.5 - z_2$, and three different reference undercoolings ΔT_0, as indicated in the graphs. The excess energy parameters are taken equal to $\phi_{12}^{s,exc} = \phi_{21}^{s,exc} = 3$. The graphs on the left give the total solid fraction s, and, in the two-phase region AB, the solid fractions s_1 and s_2 with $s = s_1 + s_2$. The graphs on the right give the average mole fractions $\bar{x}_2^{sj}$ ($= 1 - \bar{x}_1^{sj}$) for each of the solid phases.

with a liquid and two solid phases at a given temperature, we have a eutectic line according to the Gibbs phase rule. Then the end point of the crystallization, which lies on this line, can vary depending on the crystallization path, which in turn depends on the evolution of the growth surfaces. This explains the small difference in the total solid fraction for the ternary system.

We have also done calculations for other values of the parameters g and ν. If we take ν larger than 0.01 (and smaller than 1), while keeping g equal to 1, the results get closer to those using the "no-history model". This is to be expected, because a larger ν means a more easy nucleation of one solid phase onto the other, so that the retardation effect induced by a slowly evolving growth surface is reduced. On the other hand, taking $\nu < 0.01$ did hardly change the results anymore, and so in this sense the results in Figure 3 represent extreme cases. Increasing (decreasing) g has a very similar effect as increasing (decreasing) ν. Reducing g leads to a retardation in the evolution of the growth surface, while a large g yields results that are closer to those using the "no-history model".

4. Kinetic vs Equilibrium Phase Separation

The final, metastable state according to the kinetic model can be charaterized by the solid fractions $s_{j,ms}$ ($j = 1, ..., N_s$) and $s_{ms} = \sum_j s_{j,ms}$, the final liquid composition $\mathbf{x}_{i,ms}^1$, the average composition(s) of the solid phase(s) $\bar{\mathbf{x}}^{sj}$ ($j = 1, ..., N_s$), and the corresponding nonhomogeneities $\Delta \boldsymbol{x}^{sj} = (\Delta x_1^{sj}, \Delta x_2^{sj}, ...)$, which are defined as the standard deviation of $\bar{\mathbf{x}}^{sj}$.[1] With this characterization we can make a study of the metastable state as a function of the overall composition or the temperature and compare it with the equilibrium state.

In Figure 4 the above characterization of the metastable state (full lines) for the binary system PPP−MyPP of section 3 with excess parameters equal to $\phi_{21}^{s,exc} = \phi_{12}^{s,exc} = 3.0$ is given as a

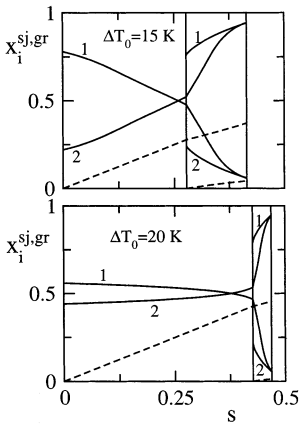

Figure 5. Crystallization curves for the binary system PPP−MyPP plus solvent with overall composition $z = (0.25, 0.25)$, $\phi_{12}^{s,exc} = \phi_{21}^{s,exc} = 3$ and two difference reference undercoolings. The dashed lines give the solid fractions $s_j(s)$.

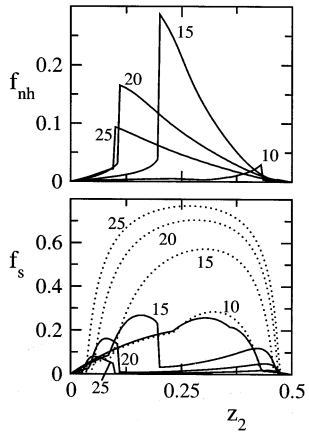

Figure 6. Total nonhomogeneity function f_{nh} (top graph) and the total segregation function f_s (bottom graph) for reference undercoolings equal to $\Delta T_0 = 10$, 15, 20, and 25 K for the same system as in Figure 4, as a function of $z_2 = 0.5 - z_1$.

function of the overall composition z_2 with a fixed solvent fraction $z_{solv} = 0.5$, together with the corresponding quantities in the calculated equilibrium state (dotted lines). In each graph, three regions (A, B, and AB) can be distinguished, separated by vertical lines. In the regions A and B the final state consists of only one solid phase, a PPP-rich and a MyPP-rich phase, respectively. In the region AB there are two coexisting solid phases. For increasing reference undercooling, ΔT_0, the width of the two-phase region and the total solid fraction increase, but the fraction of solid phase 2, s_2, decreases, as can be seen in the graphs on the left. For $\Delta T_0 = 20$ K there is one strongly dominant solid phase and only a tiny bit of a second solid phase for the entire composition range. In contrast, the equilibrium model predicts approximately equal amounts of the two solid phases at $z_2 = z_1 = 0.25$ for large ΔT_0. This difference between the predictions of the kinetic and equilibrium models, which increases for increasing ΔT_0, is also reflected in the (average) compositions of the solid phases, which are shown in the graphs on the right. For small ΔT_0, mixing is limited and the differences remain small. According to the equilibrium model mixing remains limited also for increasing undercooling ΔT_0, whereas the kinetic model predicts a strongly increased mixing, which is consistent with the fact that one solid phase is formed predominantly. For $\Delta T_0 = 20$ K, the mixing in this solid phase is almost perfect in the sense that $\bar{x}_2^{s1} \simeq z_2/(z_1 + z_2)$. This effect of the temperature is further illustrated in Figure 5, which shows the growth composition as a function of s for $z_2 = z_1 = 0.25$ and two different reference undercoolings. Lowering the temperature leads to an increasing amount of the dominant solid phase, which becomes more and more homogeneous, and a reduction of the amount of the second solid phase evolving in a later stage of the crystallization process. For $\Delta T_0 > 15$ this holds for the entire overall composition range, as can be seen in the top graph of Figure 6, which shows the total nonhomogeneity function as a function of z_2. Here we have defined the total nonhomogeneity function for a multicomponent system as a weighted sum of all standard deviations $\Delta x^{sj}{}_i$:

$$f_{nh} = \frac{1}{s}\sum_{j=1}^{N_s}\sum_{i=1}^{N_c} s_j x_i^{sj}\,\Delta x_i^{sj} \qquad (19)$$

For ΔT_0 from 10 to 15 K, the nonhomogeniety increases, however, as to compensate for a reduction in the phase separation. As a last, additional characterization of the final state we define the total segregation function, f_s, which for a multicomponent system reads

$$f_s = \frac{1}{(N_c - 1)}\sum_{j=1}^{N_s}\sum_{i=1}^{N_c} s_j(\hat{z}_i - \bar{x}_i^{sj})^2/z_i \qquad (20)$$

where $\hat{z}_i \equiv z_i/\sum_i z_i$. This function has the property that its value is equal to 1 in the limit of low temperatures (i.e., complete solidification of the crystallizing components) for complete separation of the components, i.e., when N_c pure solid phases are formed with fractions $s_j = z_j$. On the contrary, f_s is equal to 0 for complete mixing, i.e., when only one solid phase is formed with $s = \sum_i z_i$ and $\bar{x}_i^s = \hat{z}_i$. For our binary system, f_s is shown in the bottom graph of Figure 6 for both the metastable state (full lines) and the equilibrium state (dotted lines). As we can see, the effect of the undercooling is opposite for both models. According to the kinetic model, the final state rapidly tends to the completely mixed situation for increasing undercooling, in agreement with the previous discussions of Figures 4 and 5. Note also that for a given T, f_{nh} is large where f_s is small, and vice versa for the metastable state. This illustrates our previous comment immediately after eq 19.

Figures 7 and 8 show the characterizations of the metastable states for a blend with 5 and 8 components, respectively, this time as a function of temperature. The corresponding equilibrium states are given by the dotted lines. The thermodynamic data for these blends, which we will denote as blend 1 and blend 2, with realistic values for the excess energy parameters, are given in Appendix A. Blend 1 contains a large amount of the component LLL, which has a melting temperature 89 K below that of the component with the highest melting temperature. For blend 2, the range of melting temperatures is only 19 K.

As shown in the top graph of Figure 7, for blend 1 the metastable state consists of only one solid phase over the entire temperature range. Contrary, the equilibrium model predicts a region with one solid phase and a region, below $T \simeq 270$ K, with two solid phases. At the lowest temperatures in this graph these are roughly speaking a LLL-rich (5) solid phase, with the highest solid-phase fraction, and a LaLaS-rich (3) solid phase, as can be seen in the middle graph, where the average mole fractions of the components 1, 3, and 5 in solid phases are drawn. The separation of these components is due to the relative high excess parameters $\phi_{35}^{s,exc} = \phi_{53}^{s,exc}$. Above $T \simeq 270$ K there is hardly any difference between the results from the kinetic

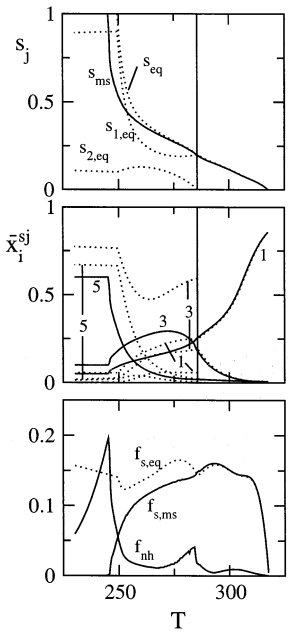

Figure 7. Characterization of the metastable (full curves) and the equilibrium states (dotted curves) for blend 1 with five components as specified in Appendix A, as a function of the crystallization temperature T_{cr}. The top graph gives the total solid-phase fraction s_{ms} and s_{eq} and the solid-phase fractions for each of the two solid phases occurring in the equilibrium state, $s_{1,eq}$ and $s_{2,eq}$. The middle graph gives the average mole fractions of the components 1 (PSS), 3 (LaLaS), and 5 (LLL) in each of the solid phases. Each of these three components occurs as the dominant component but in different temperature regions.

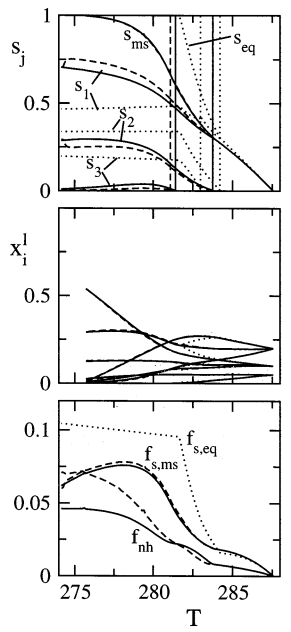

Figure 8. Characterization of the metastable (full curves) and the equilibrium states (dotted curves) for blend 2 with eight components specified in Appendix A, as a function of T_{cr}. The middle graph gives the mole fractions in the final liquid phase.

and equilibrium models. Below that temperature a second, LaLaS-rich solid phase starts to come up according to the equibrium model. In contrast, according to the kinetic model, the increasing affinity of this component to crystallize as the temperature decreases does not give rise to phase separation but is reflected in an increasing average concentration of that component in the solid phase. The total solid-phase fraction is very similar for both models, except for a small range of temperatures yielding a high solid-phase fraction around $T =$ 250 K. For this blend, where a large spread in the pure component melting temperature exists, the solid-phase fraction is mainly determined by the affinity of each of the individual components to crystallize, which is to a certain extent independent of the kinetics. The onset of the difference in the phase separation behavior, as characterized by total segregation functions $f_{s,ms}$ and $f_{s,eq}$, shown in the bottom graphs, occurs at the temperature which separates the one-phase region and the two-phase region according to the equilibrium model. This difference increases for lower temperatures. Note that $f_{s,ms} = 0$ at $T \simeq 245$ K, where $s_{ms} = 1$, as it should be for the case with only one solid phase and no liquid according to the definition of f_s (eq 20). The large difference in the solid-phase fraction at T around 250 K is accompanied by a large inhomogeneity, as can be seen in the bottom graph, where we have plotted the total nonhomogeneity function f_{nh}. This is caused by the increasing affinity of the low melting temperature component LLL to crystallize when the temperature is lowered. However, the high melting components will crystallize first, so that there is a strong variation in the growth composition.

In contrast to blend 1, for blend 2 kinetic phase separation occurs, as shown in Figure 8. The difference in the total solid phase fraction is clearly more significant than for blend 1 (top graph). The equilibrium model predicts a completely solidified state (i.e., $s = 1$) for T below ~283 K, whereas for the kinetic model this state is only reached for T below ~277 K, which is a relatively large difference compared to the melting range. There are three different temperature regions, with one, two, and three solid phases, for both models. However, the vertical lines that mark these regions are shifted to lower temperatures for the kinetic model relative to those for the equilibrium model. In addition, as can be seen most clearly in the three-phase region, the first solid phase has become more dominant for the kinetic model, i.e., $s_{1,ms} > s_{1,eq}$, leading to a reduction of the two other phases (see top graph). This tendency, which was also observed previously for the binary system, is even stronger if the growth surface model eq 18 is used (dashed lines) instead of the "no-history model" (full lines). The required formation of growth surface for the second and third solid phases leads to a retardation in the growth of these solid phases, implying a reduction of the solid-phase fractions for these phases in the end. Nevertheless, the differences in the solid fractions that occur for the different treatments of the growth surface problem are again rather small, regardless of the values of the parameters g and ν. This holds also for the total average solid phase composition (i.e., averaged over all solid phases), as can be concluded by combining total mass balance with the fact that both the total solid phase fraction and the final liquid composition (middle graph) are practically equal. The difference in the nonhomogeneity function is more significant (bottom graph). If the second solid phase is hindered to grow due to absence of growth surface, then the dominant components of this solid phase, which somehow have a relatively large affinity to crystallize, start to co-crystallize with the first solid phase, leading to an enhanced inhomogeneity. The kinetically induced reduction of the phase separation with respect to the equilibrium state is clearly reflected by the total segregation functions and are very similar for the two growth surface models.

5. Summary and Conclusions

Using a previously introduced kinetic model,[1] which has been extended with an equation describing the evolution of the growth

surfaces, we find that phase separation during growth from the liquid in mixed systems is reduced kinetically in a specific way. As a function of increasing undercooling, one of the solid phases becomes more and more dominant, although this phase may be strongly inhomogeneous within a certain range of crystallization temperatures. In the low-temperature limit, kinetic phase separation vanishes and we find a homogeneous solid phase. Significant differences in the total solid-phase fraction and the phase separation behavior occur at crystallization temperatures yielding high solid-phase fractions. As in the case without phase separation,[1] the solid-phase fraction of the metastable state resulting from the kinetic model can be much lower than the equilibrium value.

The proposed growth surface model contains two parameters that regulate the evolution of the growth surfaces as a function of the differences in growth rates and of the heterogeneous nucleation, respectively. However, the influence of these parameters on the final state appears to be rather small due to an intrinsic stabilizing mechanism in the equations. If the formation of one of the solid phases is hindered by the lack of growth surface for this phase, then the supersaturation for this phase will increase relative to that of the other solid phases, favoring the nucleation, subsequent growth, and formation of growth surface for this phase. This explains why even the most simple approach for the growth surface problem, where the growth fractions are given by the ratio of the instantaneous growth rates for the different solid phases ("no-history model"), still gives similar results.

In this paper we have compared the results of our kinetic model with those from the standard equilibrium approach. From the experimental side, information about the phase separation behavior can be obtained by differential scanning calorimetry (DSC) measurements. Due to kinetics, the melting DSC curve depends on the conditions at which the crystallization has taken place.[22] Future work will deal with the quantitative connection between our calculations and DSC data from specific experiments to be done.[23] In this context we also intend to investigate the role of mass and heat diffusion and incorporate these processes within the present type of description.

Acknowledgment. This work has been sponsored by Unilever Research Vlaardingen, The Netherlands. We thank Prof. T. Janssen, Dr. A. Fasolino, and Dr. B. Polman for discussions and assistance.

Appendix A

The melting temperatures and melting heats of the pure components PPP, MyPP, and SOS, used in section 3, are $T_i =$ 337.50, 330.96, and 317.90 K and $\Delta H_i =$ 169.04, 148.22, and 134.87 kJ/mol, respectively. Here, a convential nomenclature is used for fat components (triglyceride). La, My, P, S, and O represent the fatty acids that are esterified with the glycerol and stand for lauric, myristic, palmitic, stearic, and oleic acid with chain lengths of 12, 14, 16, 18, and 18 carbon atoms, respectively.

The tables below contain the thermodynamic data for the β'-phase of blend 1 and blend 2 used in section 4. Also included

TABLE 1: Blend 1

	PSS	LaSS	LaLaS	LLS	LLL
z_i	0.049	0.096	0.105	0.141	0.609
T_i	334.16	321.79	315.21	273.96	245.10
ΔH_i	152.63	91.83	57.75	43.04	38.39
$\phi_{1i}^{s,exc}$	0.000	0.325	3.340	0.000	0.000
$\phi_{2i}^{s,exc}$	0.325	0.000	1.480	1.140	1.140
$\phi_{3i}^{s,exc}$	3.340	1.480	0.000	0.000	4.270
$\phi_{4i}^{s,exc}$	0.000	1.140	0.000	0.000	0.000
$\phi_{5i}^{s,exc}$	0.000	1.140	4.270	0.000	0.000

TABLE 2: Blend 2

	PMyO	POP	PLaO	LaOP	OOA	OOS	LaLP	POO
z_i	0.20	0.05	0.20	0.20	0.10	0.10	0.10	0.05
T_i	303.11	300.15	298.76	297.60	296.03	292.31	286.75	284.15
ΔH_i	42.09	98.52	34.25	42.08	61.90	69.06	30.00	65.48
$\phi_{1i}^{s,exc}$	0.00	1.34	0.00	3.44	2.05	1.24	3.44	0.43
$\phi_{2i}^{s,exc}$	1.34	0.00	2.35	0.50	1.14	0.36	0.50	0.00
$\phi_{3i}^{s,exc}$	0.00	2.35	0.00	4.65	3.04	2.19	4.65	1.34
$\phi_{4i}^{s,exc}$	3.44	0.50	4.65	0.00	3.04	2.19	0.00	1.34
$\phi_{5i}^{s,exc}$	2.05	1.14	3.04	3.04	0.00	0.00	3.04	0.30
$\phi_{6i}^{s,exc}$	1.24	0.36	2.19	2.19	0.00	0.00	2.19	0.00
$\phi_{7i}^{s,exc}$	3.44	0.50	4.65	0.00	3.04	2.19	0.00	1.34
$\phi_{8i}^{s,exc}$	0.43	0.00	1.34	1.34	0.30	0.00	1.34	0.00

are the dimensionless excess energy parameters $\phi_{ii'}^{s,exc}$ and the overall mole fractions z_i. All thermodynamic data are taken from ref 5.

References and Notes

(1) Los, J. H.; van Enckevort, W. J. P.; Vlieg, E.; Flöter, E. *J. Phys. Chem. B*, **2002**, *106*, 7321.
(2) Michelsen, M. L. *Fluid Phase Equilib.* **1982**, *9*, 1. Michelsen, M. L. *Fluid Phase Equilib.* **1982**, *9*, 21.
(3) de Bruyne, P. et al., *Chem. Phys. Lipids* **1972**, *9*, 309.
(4) Ollivon, M.; Perron, R. *Chem. Phys. Lipids* **1979**, *25*, 395.
(5) L. H. Wesdorp, Liquid-multiple solid-phase equilibria in fats. Ph.D. Thesis, University Delft, The Netherlands, 1990.
(6) Timms, R. E. *Prog. Lipid Res.* **1984**, *23*, 1.
(7) Los, J. H.; Flöter, E. *Phys. Chem. Chem. Phys.* **1999**, *1*, 4251.
(8) *Kinetic Phase Diagrams*; Chvoj, Z.; Šesták, J.; Tříska, A., Eds.; Elsevier: Amsterdam, 1991.
(9) Pfeiffer, H.; Haubenreisser, W. *Phys. Status Solidi B* **1980**, *101*, 253.
(10) Cherepanova, T. A. *J. Cryst. Growth* **1980**, *59*, 371.
(11) Cherepanova, T. A.; Didrikhsons, G. T. *Phys. Status Solidi A* **1980**, *59*, 633.
(12) Ginzburg, V. V. *Phys. Rev. B* **1999**, *60*, 4352.
(13) Orlikowski, D.; Sagui, C.; Somoza, A.; Roland, C. *Phys. Rev. B* **1999**, *59*, 8646.
(14) Sharma, F.; Puri, S. *Phys. Rev. E* **2001**, *64*, 021513.
(15) Soisson, F.; Martin, G. *Phys. Rev. B* **2000**, *62*, 203.
(16) Gilbert, E. P.; Reynolds, P. A.; Brown, A. S.; White, J. W. *Chem. Phys. Lett.* **1996**, *255*, 373.
(17) Dorset, D. L.; Snyder, R. G. *J. Phys. Chem. B* **1999**, *103*, 3282.
(18) Knoester, M.; de Bruyne, P.; v.d. Tempel, M. *J. Cryst. Growth* **1968**, *3*, 776.
(19) van Putte, K. P. A. M.; Bakker, B. H. *Jaocs* **1987**, *64*, 1138.
(20) Prausnitz, J. M. *Molecular Thermodynamics of Fluid Phase Equilibria*; Prentice Hall: Englewood Cliffs, NJ, 1986.
(21) Oonk, H. A. J.; Mondieig, D.; Haget, Y.; Cueveas-Diarte, M. A. *J. Chem. Phys.* **1998**, *108*(2), 715.
(22) van Genderen, A. C. G.; de Kruif, C. G.; Oonk, H. A. J. *Z. Phys. Chem. Neue Folge* **1977**, *107*, 167.
(23) J. H. Los et al., work in progress.